Biointerface Research in Applied Chemistry
Open-Access Journal (ISSN: 2069-5837)

Article
Volume 16, Issue 2, 2026, 45
https://doi.org/10.33263/BRIAC162.045

Integrative Network Pharmacology, Molecular Docking, and Dynamics Analysis of Rhizomes for Prevention of Sarcopenia

Fathir Azzaki Iradata [1], Ahmad [1], Firdayani [2], Irma Ratna Kartika [1], Danang Waluyo [2], Titin Ariyani [2], Erwahyuni Endang Prabandari [2], Nuki Bambang Nugroho [2], Muthia Rahayu Iresha [2,*]

[1] Chemistry Study Program, Faculty of Mathematics and Natural Sciences, State University of Jakarta (UNJ), Rawamangun, East Jakarta, Jakarta 13220, Indonesia
[2] Research Center for Vaccines and Drugs, Research Organization for Health, National Research and Innovation Agency (BRIN), Cibinong, Bogor, West Java 16915, Indonesia
* Correspondence: muth005@brin.go.id;

Received: 10.11.2025; Accepted: 4.02.2026; Published: 15.04.2026

Abstract: Sarcopenia is a condition that is characterized by a gradual decline in skeletal muscle mass, strength, and function. Abundant bioactive compounds in jamu, a traditional Indonesian herbal, can reduce oxidative stress and inflammation while improving physical performance and muscle health. The present study aims to uncover the active compounds in *Zingiber officinale* (red ginger), *Kaempferia galanga* (aromatic ginger), and *Curcuma sp.*, and elucidate their potential mechanisms for preventing sarcopenia. A total of 41 phytochemicals (15 from *Z. officinale*, 11 from *Curcuma sp.*, and 15 from *K. galanga*) were selected from the literature. Network pharmacology analysis identified AKT1, TP53, and BCL2 as the targets with the highest degree values. Molecular docking showed Curcumin exhibited the strongest binding affinity toward AKT1 (re-rank score: -117.897), while 1-dehydro-10-gingerdione showed the highest affinities for both TP53 (re-rank score: -117.595) and BCL2 (re-rank score: -85.1227). The molecular dynamics simulation showed that the Curcumin–AKT1 complex has similar stability to the native–AKT1 complex, with an average RMSD backbone profile of 2.98 Å, SASA of 18,655 Å^2, and RMSF of 1.23 Å. This study suggests that the three rhizome-derived compounds may be potential anti-sarcopenia agents, though this will require future experimental validation. The research also establishes a framework for investigating how the three rhizomes might influence the PI3K-Akt pathway and endocrine resistance.

Keywords: sarcopenia; network pharmacology; molecular docking; ADMET; molecular dynamics simulation.

1. Introduction

Sarcopenia is a progressive condition marked by the decline of skeletal muscle mass, strength, and function, presenting a significant health challenge, particularly in older adults. Its multifactorial etiology includes aging, hormonal changes, nutritional deficiencies, physical inactivity, chronic inflammation, and oxidative stress, all of which contribute to muscle degeneration and functional impairment [1–3]. The prevalence of sarcopenia is substantial, affecting 16.5% of community-dwelling older adults, with higher rates in those 60-80 years,

and is projected to rise as the global population over 60 is expected to reach 2.1 billion by 2050 [4–6]. This increase underscores the urgent need for effective strategies to prevent muscle loss and its associated morbidity.

Traditional Indonesian herbal medicine, known as Jamu, employs rhizomatous plants such as *Zingiber officinale* (red ginger), *Kaempferia galanga* (aromatic ginger), and *Curcuma sp.*, to alleviate musculoskeletal discomfort, combat fatigue, and enhance physical endurance. Preclinical studies indicate that these herbs can enhance muscle mass, improve endurance, reduce muscle atrophy, and improve stamina [7–9]. Despite the well-documented traditional use of these rhizomes, there is limited discussion on their specific selection for sarcopenia-related mechanisms.

According to reports, *Z. officinale* extract reduces pro-inflammatory biomarkers and oxidative stress, supporting muscle mass and strength by modifying these pathological pathways [10]. The main component of *Curcuma sp.*, Curcumin, prevents inflammatory cascades associated with muscle atrophy [11]. Similarly, ethyl-p-methoxycinnamate from *K. galanga* exhibits antioxidant and anti-inflammatory properties, including the inhibition of nitric oxide and IL-6 synthesis [12]. Despite their widespread use, a systematic evaluation of their mechanisms in relation to sarcopenia remains limited.

Network pharmacology has emerged as a popular tool for investigating multi-component herbal remedies by constructing "protein-compound/disease-gene" networks and predicting biological targets and mechanisms [13]. Complementary computational approaches, including molecular docking, ADMET prediction, and molecular dynamics simulation, enable a detailed analysis of ligand-protein interactions and the dynamic stability of complexes over time [14–16].

The present study employs an integrative framework combining network pharmacology, molecular docking, and molecular dynamics simulation to identify active compounds from these rhizomes and elucidate their potential mechanisms for preventing sarcopenia. This research aims to identify new therapeutic candidates that may slow down muscle degeneration and improve musculoskeletal health in aging populations by integrating traditional herbal knowledge with computational techniques.

2. Materials and Methods

2.1. Screening of active compounds.

Chemical information was obtained from published literature to identify the major bioactive compounds present in *Z. officinale*, *Curcuma sp.*, and *K. galanga* [17–22]. The literature review involved an examination of various scientific sources, including research journals from reputable databases.

2.2. Target collection and potential target prediction.

The investigation commenced by curating the chemical structures of *Z. officinale, Curcuma sp.,* and *K. galanga* bioactive compounds, represented as Simplified Molecular Input Line Entry System (SMILES) notations. Several integrative software, such as Swiss Target Prediction (http://www.swisstargetprediction.ch/) (SIB Swiss Institute of Bioinformatics, Lausanne, Switzerland) [23], Way2Drugs PASS online (http:// https://www.way2drug.com/passtargets/) (Institute of Biomedical Chemistry, Moscow, Russia) [24], and STITCH (http://stitch.embl.de/) (Max Planck Institute for Molecular Cell

Biology and Genetics, Dresden, Germany) [25], were used by employing different prediction techniques to collect the putative target prediction (genes) of the active compounds relating to sarcopenia. All accessible targets were restricted to *Homo sapiens*.

The protein targets associated with sarcopenia were identified through a search using the keyword "sarcopenia" in both the GeneCard database (https://www.genecards.org/) (Weizmann Institute of Science, Rehovot, Israel) [26] and the STRING database (https://string-db.org/) (SIB Swiss Institute of Bioinformatics, Lausanne, Switzerland) [27]. Duplicated targets were excluded.

2.3. Network formation and validation.

Venn diagrams were used to identify the similar genes between sarcopenia targets and compound targets (https://bioinfogp.cnb.csic.es/tools/venny/) (Centro Nacional de Biotecnología, Madrid, Spain) [28]. The intersected target genes were subsequently imported into the STRING database to construct a Protein–Protein Interaction (PPI) network, which was then visualized and analyzed using Cytoscape version 3.10.3 (National Human Genome Research Institute, Maryland, United States) [29].

2.4. Pathway and functional enrichment analysis.

GO enrichment analysis (Molecular Function–MF, Biological Process–BP, and Cellular Component–CC) and KEGG pathway annotation were carried out using ShinyGO 0.77 (http://bioinformatics.sdstate.edu/go/) (South Dakota State University, South Dakota, United States) [30]. Intersection target proteins of sarcopenia and the active compound of *Z. officinale*, *Curcuma sp.*, and *K. galanga* served as input, with the species "Human", False Discovery Rate (FDR) cutoff at 0.05, and display of 30 pathways [31]. The GO functions were visualized using a histogram bar plot, and the resulting pathways were correlated with sarcopenia.

2.5. Molecular docking.

Molecular docking analysis was conducted in a single run using Molegro Virtual Docker 6.0 (MVD) (Molexus ApS, Odder, Denmark) [32]. The top three hub genes were selected as target proteins based on their centrality in the PPI network. Degree centrality was used as the selection criterion to prioritize proteins with extensive interaction profiles, which are considered potential key targets. The three-dimensional (3D) crystal structures of target proteins were retrieved from the RCSB Protein Data Bank (PDB) (https://www.rcsb.org) (RCSB, San Diego, California, USA) [33]. The selection of protein structures was based on atomic resolution, the availability of protein-ligand complexes, active site residues, and the organism source. The protein structures were prepared by removing water molecules, ions, and nonessential cofactors. The chemical structures of those compounds were retrieved using the PubChem database (https://pubchem.ncbi.nlm.nih.gov/) (National Library of Medicine, Bethesda, Maryland, USA) [34]. The 3D ligand structures of secondary metabolites were generated using ChemOffice (https://www.perkinelmer.com) and subjected to energy minimization using the Merck Molecular Force Field 94 (MMFF94) [35]. The optimized ligand structures were saved in MOL2 format and subsequently imported into MVD for docking simulations. To validate the docking procedure, we redocked the native ligand into the active site of the respective target protein to ensure structural fidelity and accurate binding

conformation. The docking grid was defined by centering it on the binding site of the co-crystallized native ligand, thereby preserving the biologically relevant interaction region and enabling reliable validation through redocking. Docking simulations were performed using the Molegro Virtual Docker scoring function, yielding 10 docking poses per ligand. The best pose, determined based on the lowest re-rank score, was selected for further analysis. Post-docking interaction analyses were conducted using BIOVIA Discovery Studio Visualizer v24.1.0 (Dassault Systèmes, Paris, France) to evaluate hydrogen bonding, hydrophobic interactions, and π-π stacking interactions between the ligands and target proteins [36].

2.6. Drug-likeness and ADMET parameters.

The structure of the selected rhizome-derived compounds with the highest re-rank score for each enzyme was further investigated using the ADMET and Lipinski rule of five. Their canonical SMILES representations were input into ADMETlab 3.0 (https://admetmesh.scbdd.com) and the pkCSM online tool (http://biosig.unimelb.edu.au/pkcsm/prediction) for ADMET profiling [37,38]. The key ADMET parameters that were assessed include Human Intestinal Absorption (HIA), Caco-2 cell permeability, Steady-State Volume of Distribution (VD_{ss}), Blood–Brain Barrier (BBB) permeability, CYP2D6 and CYP3A4 substrate classification, total clearance, and toxicity.

2.7. Molecular dynamics simulation.

Molecular Dynamics (MD) simulations were conducted using GROMACS 2023 (https://www.gromacs.org/) [39] on the MAHAMERU High-Performance Computing (HPC) system, operated by the National Research and Innovation Agency of Indonesia (BRIN). The protein topology was written by pdb2gmx using the CHARMM36-jul2022 [40] force field and the TIP3P original water model [41] (http://mackerell.umaryland.edu/charmm_ff.shtml#gromacs). The protein structure was preprocessed by removing water molecules and reference ligands, and its topology was generated accordingly. The three best secondary metabolites from molecular docking studies were used as ligands. Ligand topologies were prepared by adding hydrogen atoms and converting the structure to mol2 format using OpenBabel (https://www.cheminfo.org/), before processing through the CHARMM General Force Field (CGenFF) server (https://app.cgenff.com/) [42,43] for topology generation. The CGenFF files were converted to GROMACS-compatible formats using the cgenff_charmm2gmx_py3_nx2.py script, ensuring compatibility with the CHARMM36 force field [44]. The resulting ligand parameter files included bonded terms (bond lengths, angles, and dihedrals), nonbonded Lennard-Jones parameters, and partial atomic charges derived from the CGenFF charge model. The protein-ligand complex was assembled, solvated in a rhombic dodecahedral box, and neutralized with Na^+ and Cl^- ions by replacing some water molecules. Energy minimization was achieved using the steepest descent algorithm until the maximum force was less than 1,000 kJ mol^{-1} nm^{-1}. System equilibration was carried out in two phases: an isothermal-isochoric ensemble (NVT) and an isothermal-isobaric ensemble (NPT). After the system was well equilibrated at 300 K and 1 bar, a 300 ns MD production run was conducted under NPT conditions.

The MD simulation trajectories were recentered and rewrapped within the rhombic dodecahedral box using the gmx trjconv module with Periodic Boundary Condition (PBC) correction and the nojump option to eliminate artifacts from molecules crossing the box

boundary. The gmx rms module was used to compute the Root Mean Square Deviation (RMSD) for comparing each structure from a trajectory to the energy minimization result structure. The Solvent-Accessible Surface Area (SASA) was calculated with the gmx sasa module to assess changes in protein surface exposure upon ligand binding. In addition, the Root Mean Square Fluctuation (RMSF) of the residue position in the trajectory after fitting to the energy-minimized frame was analyzed with the gmx rmsf module.

3. Results and Discussion

3.1. Screening of active components.

A total of 41 major compounds from *Z. officinale*, *Curcuma sp.*, and *K. galanga* were identified through a comprehensive review of the literature and database screening using Google Scholar and PubChem (accessed January 2025). Compounds were selected based on their reported abundance and biological relevance, with particular emphasis on sarcopenia-related pathways. The identified compounds are summarized in Table 1.

Table 1. Major rhizome compounds collected from the literature.

Plants sources	Compounds	References
Z. officinale	6-Gingerol	[17]
	6-Shogaol	
	Gingerenone A	
	1-Dehydro-10-gingerdione	
	Gingerdione	
	Zingerone	
	6-Paradol	
	8-Gingerol	[18]
	10-Gingerol	
	α-Zingiberene	
	α-Curcumene	
	Neral	
	Geraniol	
	β-Bisabolene	
	β-Sesquiphelandrene	
Curcuma sp.	Turmerone	[19]
	Curlone	
	Curcuphenol	
	Curcumin	
	Demethoxycurcumin	
	Bisdemetoxycurcumin	
	Cyclocurcumin	
	Xanthorizol	[20]
	Camphor	
	Zerumbone	
	Geranyl acetate	
K. galanga	Pentadecane	[21]
	Ethyl p-methoxycinnamate	
	Phenyl propenoic acid	
	3,6-Nonadienal	
	8-Heptadecane	
	γ- Murolene	
	Cyperene	
	α -Gurjunene	
	Palmitic acid	[22]
	Capric acid	
	Caprylic acid	
	Lauric acid	
	Stearic acid	
	Myristic acid	
	γ-Palmitolactone	

3.2. The PPI network and the ‘‘herbs-components-targets-disease” network.

A total of 445 potential targets were identified as being associated with 41 main compounds from the search using SwissTargetPrediction and Way2Drugs. Sarcopenia-related targets were identified from the GeneCards database, yielding 297 targets, and from the STRING database, yielding 50 targets. After eliminating duplicates and integrating the sarcopenia-associated targets, researchers identified 37 common targets that represent key intersections between compound-related targets and sarcopenia-related pathways (Figure 1a). A PPI network was constructed to elucidate the complex interactions among these targets (Figure 1b).

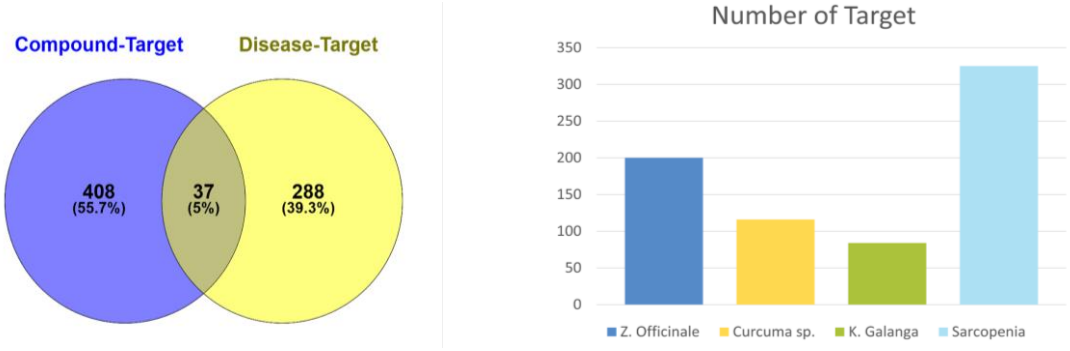

(a) **(b)**

Figure 1. Predicted gene targets of rhizome-derived compounds. (**a**) Venn diagram showing overlapping and unique predicted genes among datasets; (**b**) Number of predicted target proteins associated with compounds from each rhizome.

The PPI network for the 37 common targets was constructed using the STRING database and visualized in Cytoscape to determine their total degree, closeness, and betweenness centrality values, illustrating the proteins with the most significant impact within this network. To identify key hub genes, the CytoHubba plugin was utilized, and the degree method was selected for ranking hub genes based on their connectivity. The top-ranked hub genes identified were AKT1 as the most central node, followed by TP53 and BCL2 (Figure 2).

These compounds are closely associated with the PI3K-Akt pathway, particularly involving AKT1 proteins, which exhibit the highest degree values. The PI3K-Akt pathway plays a crucial role in maintaining muscle mass, as it can both promote protein synthesis by activating mTOR and inhibit protein degradation by blocking FoxO-mediated transcription of muscle atrophy genes, such as Atrogin-1 and MuRF1 [45]. In sarcopenia, the PI3K-Akt pathway is often downregulated due to age-related insulin resistance and inflammation, resulting in impaired muscle regeneration, increased proteolysis, and progressive muscle wasting [46]. The involvement of TP53 and BCL2 further supports the notion that sarcopenia is not merely a metabolic condition, but also involves the complex regulation of cell death and repair, aligning with studies linking mitochondrial dysfunction and apoptosis to muscle degeneration in aging populations. TP53 plays dual roles in skeletal muscle: under basal or transient stress conditions, it contributes to genomic stability and mitochondrial quality control, whereas under chronic or excessive stress associated with aging, it promotes apoptosis and muscle fiber loss. Similarly, BCL2 regulates myofiber survival by inhibiting apoptosis and may also influence muscle regeneration dynamics [47,48]. These suggest potential multitarget mechanisms of the rhizome’s compound in mitigating muscle degeneration through pathways involving protein synthesis (AKT1), cell survival (BCL2), and apoptosis regulation (TP53).

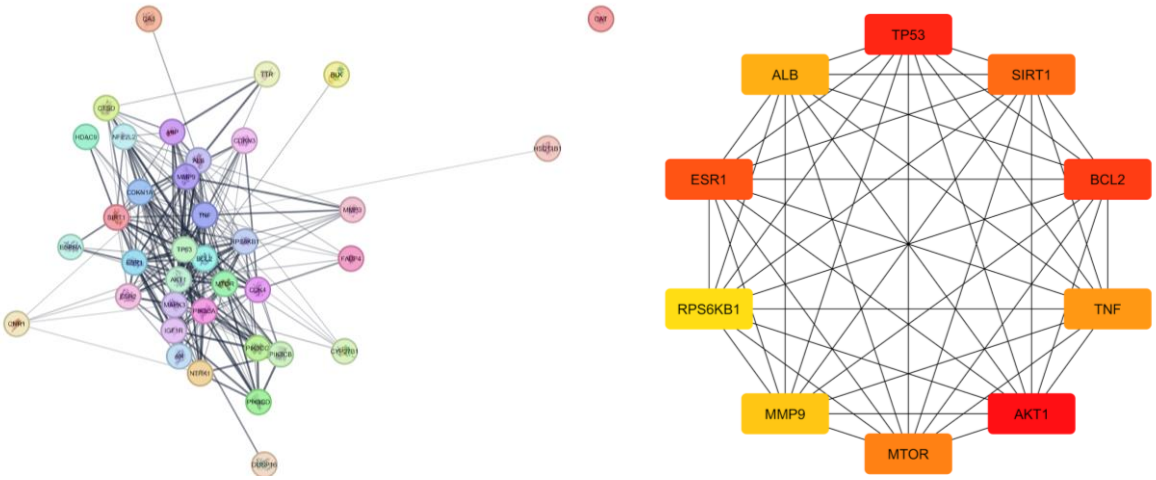

Figure 2. The PPI network and hub gene analysis. (**a**) PPI network of 37 predicted target genes, where nodes represent proteins and edges indicate interactions; (**b**) Top 10 hub genes ranked based on maximal clique centrality (MCC) scores.

3.3. Gene ontology and KEGG pathway.

The intersection target proteins were analyzed using ShinyGo 0.77 by inputting 37 target proteins, specifying the species as "human", and setting the FDR cutoff at 0.05. GO enrichment was performed, including GO BP, GO MF, and GO CC.

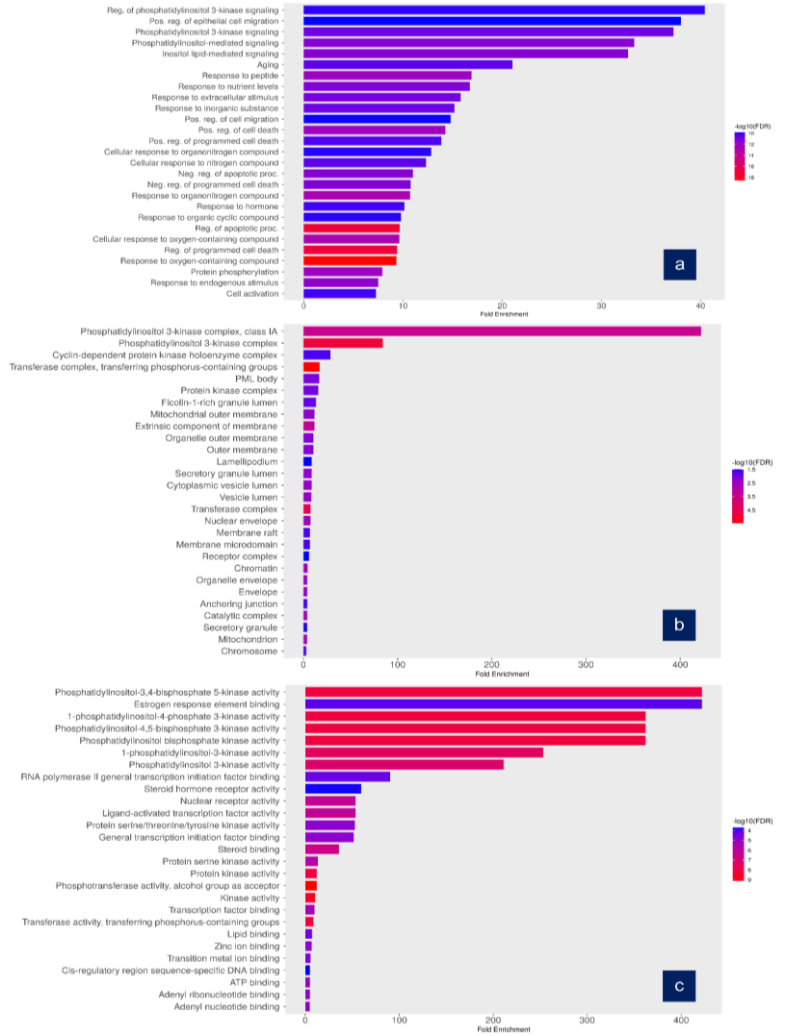

Figure 3. GO enrichment analysis of predicted target genes. Top 30 enriched GO terms categorized into (**a**) Biological Process (BP); (**b**) Cellular Component (CC); (**c**) Molecular Function (MF).

The GO enrichment results were in the 1000 BP pathway, 129 CC pathway, and 235 MF pathway. The top 30 of each GO pathway are shown in Figure 3. GO enrichment analysis revealed that the major BPs were the regulation of PIP3K signaling and the positive regulation of epithelial cell migration. The integral component of the PIP3K complex was the major CC. PIP3K activity was the primary MF. The KEGG enrichment analysis revealed that endocrine resistance was the primary pathway associated with the 37 targets, as indicated by the fold enrichment (Figure 4a), and it also exhibited the lowest FDR enrichment value (FDR < 0.05) (Figure 4b).

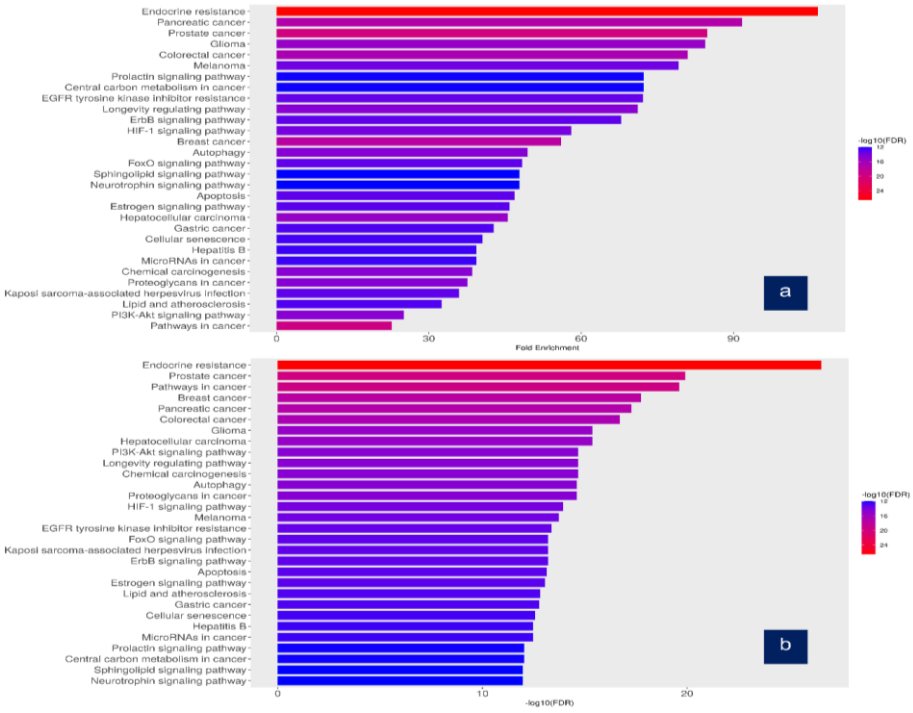

Figure 4. KEGG pathway enrichment analysis of predicted target genes. Enriched KEGG pathways are presented based on (**a**) fold enrichment; (**b**) false discovery rate (FDR).

KEGG pathways also highlight the involvement of endocrine resistance, which arises from disruptions in hormonal signaling pathways that regulate muscle metabolism, growth, and homeostasis. They are significantly pertinent to the pathology of sarcopenia. Insulin resistance impairs glucose uptake and protein synthesis in skeletal muscle, leading to muscular atrophy. This is a prevalent characteristic of sarcopenia, particularly in relation to metabolic diseases such as diabetes and obesity [49,50]. Decreased IGF-1 signaling, essential for muscle development and regeneration, is linked to sarcopenia. The PI3K/AKT pathway, which is downstream of IGF-1, frequently exhibits diminished responsiveness in older muscles, hence contributing to anabolic resistance [51]. This hormonal insensitivity creates a hormonal and inflammatory environment that accelerates muscle atrophy and drives the progression of sarcopenia. These results are in line with earlier experiments that demonstrated specific supplements enhance insulin sensitivity, reduce mitochondrial damage, increase muscle mass and strength, and upregulate proteins involved in the PI3K/Akt pathway [52,53].

3.4. Docking validation.

The top three ranked hub genes, AKT1 (PDB ID: 4GV1), TP53 (PDB ID: 6SI3), and BCL2 (PDB ID: 2W3L), were identified as the target receptors more likely to represent functionally critical intervention points [54–57]. Each native ligand was re-docked into the

protein binding site, successfully replicating the co-crystalized complex, confirming the accuracy of the docking method. The RMSD was used to evaluate the accuracy of the docking setup, where an RMSD value of less than 2Å is considered acceptable [57]. The optimized docking parameters were used as references for the docking stage of the bioactive compounds. The RMSD results from re-docking validation are shown in Table 2.

Table 2. Docking validation results of AKT1, TP53, and BCL2.

Protein Target	Center Grid Box	Radius (Å)	RMSD (Å)
AKT1	X: -19.92 Y: 4.31 Z: 11.28	12	0.9
TP53	X: 91.65 Y: 95.14 Z: -43.63	10	0.4
BCL2	X: 39.47 Y: 27.06 Z: -12.37	12	0.4

3.5. Molecular docking.

Molecular docking simulations were conducted on bioactive compounds from *Curcuma sp.*, *Z. officinale*, and *K. galanga* against AKT1, TP53, and BCL2. Docking poses were ranked using the re-rank score generated by Molegro Virtual Docker (MVD) as an initial metric to prioritize ligand-protein interactions (Table 3). The re-rank score re-evaluates docking poses using a refined energy function that incorporates van der Waals, electrostatic, hydrogen-bonding, and internal-strain contributions, thereby providing a relative estimate of binding stability rather than a definitive binding affinity [58].

Table 3. Docking results of the best compounds from *Curcuma sp.*, *K. galanga*, and *Z. officinale* against AKT1, TP53, and BCL2.

Protein target	Plants	Compounds	Re-rank score (kcal/mol)	H-Bond (kcal/mol)
AKT1	-	Capivasertib (native 1)	-114.039	-4.79
	Curcuma sp.	Curcumin	-117.897	-7.65
	K. galanga	Stearic acid	-97.306	-3.71
	Z. officinale	Gingerenone A	-109.884	-6.51
TP53	-	1-[7-Bromanyl-9-[2,2,2-tris(fluoranyl)ethyl]carbazol-3-yl]-N-methylmethanamine (native 2)	-115.567	-1.81
	Curcuma sp.	Demethoxycurcumin	-116.789	-4.91
	K. galanga	γ-Palmitolactone	-95.149	-2.13
	Z. officinale	1-Dehydro-10-gingerdione	-117.595	-4.06
BCL2	-	Chlorojanerin (native 3)	-115.556	0
	Curcuma sp.	Demethoxycurcumin	-80.807	-2.07
	K. galanga	8-Heptadecane	-72.293	0
	Z. officinale	1-Dehydro-10-gingerdione	-85.123	0

Docking was performed within predefined functional regions of each target protein. Among the screened compounds, Curcumin exhibited the lowest re-rank score for AKT1, and 1-dehydro-10-gingerdione showed the most favorable score for TP53, indicating comparatively stronger predicted ligand-protein interactions at the docking-pose level. By contrast, none of the tested compounds outperformed the reference ligand in the BCL2 model, suggesting weaker predicted binding relative to the benchmark inhibitor.

Table 4. Comparative molecular interactions of top rhizome derivatives with AKT1 and its native ligand.

Compound	Interacting residues	Types of molecular interactions
Curcumin	MET 281, GLU 278, GLU 198, GLY 162, PHE 161, THR 195,	Conventional H-bond (GLU 278, GLU 198, GLY 162, PHE 161), Carbon H-bond (THR 195, GLY 294), Pi-Donor H-bond (LYS 179,

Compound	Interacting residues	Types of molecular interactions
	GLY 294, LYS 179, GLU 191, LEU 181, LYS 163	GLU 191, LYS 163), Pi-Sulfur (MET 281), Alkyl (MET 281), Pi-Alkyl (LEU 181)
Native 1	ALA 230, GLU 234, ASN 279, MET 281, GLY 157, TYR 229, VAL 164, LEU 156, LEU 181, LYS 179, ALA 177	Conventional H-bond (ALA 230, GLU 234, ASN 279, MET 281), Carbon H-bond (GLY 157, TYR 229), Pi-Sulfur (ALA 230, MET 281), Alkyl (VAL 164, MET 281), Pi-Alkyl (ALA 177, LEU 156, LEU 181, LYS 179, VAL 164, ALA 230, MET 281)

Figures 5–7 present 2D interaction diagrams illustrating the docking poses of the top-ranked ligands within the predefined cavities of each target protein. The interacting residues and non-covalent contact of the selected ligands were compared with those of the reference ligands (Tables 4–6) to assess structural similarity of the docking pose across all target receptors. In the AKT1 complexes, residues such as MET 281, LEU 181, and LYS 179 were recurrently involved in predicted ligand interactions. For TP53, overlapping residues included PRO 151, PRO 222, PRO 223, LEU 145, and VAL 147. In BCL2, residues such as MET 74, TYR 67, PHE 71, and VAL 92 contributed primarily through hydrophobic contacts, Pi-Pi stacking, and hydrogen bonding. The Curcumin–AKT1 docking pose exhibited multiple predicted hydrogen bonds and hydrophobic interactions compared with the reference ligand. Similarly, the predicted interactions of 1-dehydro-10-gingerdione with TP53 and BCL-2 indicate potential engagement of comparable binding regions at the pose level.

Table 5. Comparative molecular interactions of top rhizome derivatives with TP53 and its native ligand.

Compound	Interacting residues	Types of molecular interactions
1-Dehydro-10-gingerdione	THR 155, PRO 151, PRO 153, PRO 222, PRO 223, LEU 145, VAL 147, GLU 221, PRO 152	Conventional H-bond (THR 152), Pi-Alkyl (PRO 151, PRO 222), Alkyl (LEU 145, VAL 147, PRO 153, PRO 223), Pi-Pi (GLU 221), Unfavorable Donor-Donor (THR 152)
Native 2	LEU 257, LEU 145, VAL 147, PRO 151, PRO 222, PRO 223, SER 220, GLU 221, ASP 228	Conventional H-bond (VAL 147, SER 220), Pi-Alkyl (PRO 151, PRO 222, PRO 223), Alkyl (LEU 257, PRO 151, LEU 145), Carbon H-bond (GLU 221, SER 220, ASP 228), Halogen Bond (LEU 145)

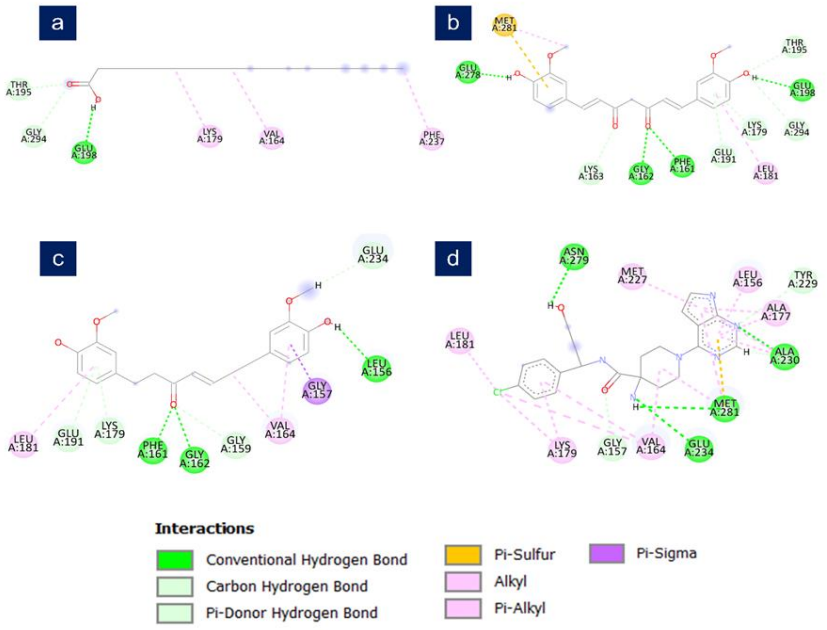

Figure 5. Molecular docking results of AKT1–ligand complexes. Predicted binding poses of AKT1 with (**a**) stearic acid; (**b**) Curcumin; (**c**) gingerenone A; (**d**) the native 1 ligand within the active site.

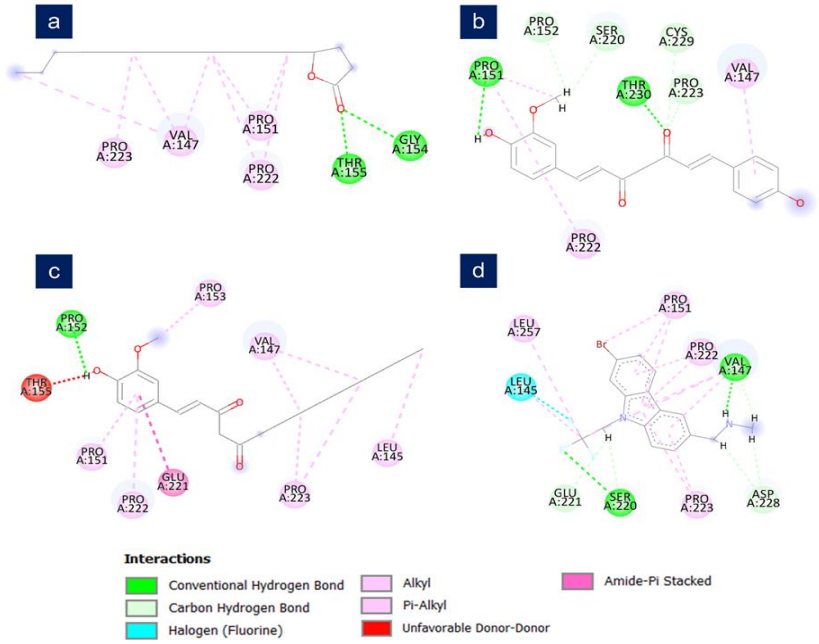

Figure 6. Molecular docking results of TP53–ligand complexes. Predicted binding poses of TP53 with **(a)** γ-palmitolactone; **(b)** demethoxycurcumin; **(c)** 1-dehydro-10-gingerdione; **(d)** the native 2 ligand.

Table 6. Comparative molecular interactions of top rhizome derivatives with BCL2 and its native ligand.

Compound	Interacting residues	Types of molecular interactions
1-Dehydro-10-gingerdione	MET 74, PHE 71, TYR 67, VAL 92, LEU 78	Carbon H-bond (MET 74, PHE 71), Alkyl (TYR 67, MET 74, VAL 92, LEU 78), Pi-Alkyl (MET 74, TYR 67) Pi-Pi (PHE 71, TYR 67)
Native 3	PHE 63, ALA 108, ARG 105, TYR 67, PHE 71, MET 74, LEU 96, VAL 92, ASP 70, GLU 95	Pi-Sigma (TYR 67, MET 74), Pi-Pi (PHE 63, PHE 71), Pi-Alkyl (ALA 108, ARG 105, MET 74, LEU 96, VAL 92), Carbon H-bond (ASP 70), Halogen bond (GLU 95), Alkyl (ARG 105, LEU 96)

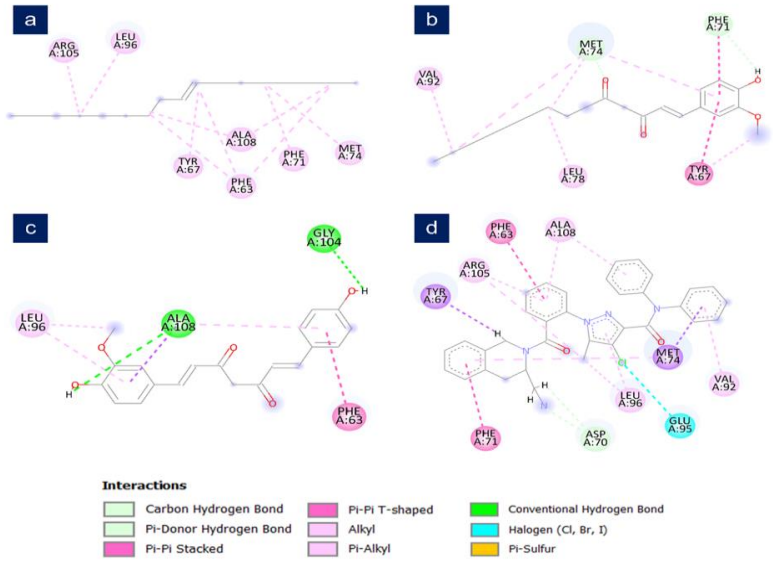

Figure 7. Molecular docking analysis of BCL2–ligand interactions. Predicted binding interactions of BCL2 with **(a)** 8-heptadecane; **(b)** 1-dehydro-10-gingerdione; **(c)** demethoxycurcumin; **(d)** the native 3 ligand.

3.6. Drug-likeness and ADMET properties.

In silico prediction of safety and pharmacokinetic properties constitutes an important step in early-stage compound prioritization. Accordingly, the pkCSM server was employed to evaluate pharmacokinetic predictions for compounds with favorable docking profiles, focusing

on compliance with Lipinski's rule of five. While the selected compounds generally adhered to established drug-likeness guidelines, Table 7 indicates that stearic acid, γ-palmitolactone, and 8-heptadecane exhibited significantly elevated lipophilicity (LogP) values. Such high lipophilicity is known to correlate with poor aqueous solubility, high metabolic turnover, and non-specific binding (pan-assay interference). Furthermore, ADMET prediction algorithms often lack reliability for such highly lipophilic, lipid-like structures. Consequently, these three compounds were excluded from further pharmacokinetic profiling to prioritize scaffolds with more favorable developability profiles. The remaining candidates—Curcumin, gingerenone A, demethoxycurcumin, and 1-dehydro-10-gingerdione—were subsequently evaluated for their detailed ADMET profiles.

Table 7. Lipinski rule of five analysis of compounds from favorable docking results.

Compound	MW	LogP	HBD	HBA	Lipinski #violations
Lipinski*	**<500**	**<5**	**<5**	**<10**	
Curcumin	368.13	2.147	2.0	6.0	0
Stearic acid	284.27	7.59	1.0	2.0	1
Gingerenone A	356.16	2.751	2.0	5.0	0
Demethoxycurcumin	338.12	2.221	2.0	5.0	0
γ-Palmitolactone	254.22	5.074	0.0	2.0	1
1-Dehydro-10-gingerdione	346.21	4.829	1.0	4.0	0
8-Heptadecane	238.27	7.931	0.0	0.0	1

Building on these physicochemical properties, further pkCSM predictions (Table 8) estimated HIA values ranging from 82.19% to 91.757% across the compounds, while most also showed predicted Caco-2 permeability values above 0.90, suggesting favorable intestinal transport potential at the computational level. Regarding metabolism, all compounds were predicted to be substrates of CYP3A4, suggesting potential involvement of cytochrome P450-mediated biotransformation. Predicted total clearance values ranged from –0.002 to 1.502 log mL/min/kg, consistent with moderate elimination profiles within the constraints of the predictive model. While these metrics indicate high oral bioavailability for the group, a distinct differentiation emerged when analyzing tissue distribution and safety parameters.

Table 8. Predicted ADMET properties of compounds from favorable docking results.

Compound	Human intestinal absorption (%)	Caco2 permeability (log Papp in 10^{-6} cm/s)	VDss (human) (log L/kg)	BBB permeability (log BB)	CYP2D6 substrate	CYP3A4 substrate	Total clearance (log mL/min/kg)	Hepato-toxicity	Oral rat acute toxicity (LD_{50})
Curcumin	82.19	-0.093	-0.215	-0.562	No	Yes	-0.002	No	1.833
Gingerenone A	91.641	0.98	0.021	-0.366	No	Yes	0.205	No	1.894
Demethoxycurcumin	91.393	1.023	-0.075	-0.337	No	Yes	0.026	No	1.973
1-Dehydro-10-gingerdione	91.757	0.486	0.389	-0.468	No	Yes	1.502	No	1.939

Although Curcumin exhibited the lowest predicted VDss (-0.215 log L/kg), it remains the most promising candidate due to its well-documented multi-target activity against inflammatory pathways relevant to sarcopenia. Its low distribution profile suggests a reduced risk of non-specific tissue accumulation and systemic toxicity. Furthermore, Curcumin demonstrated the most favorable safety profile regarding BBB permeability (log BB = -0.562), indicating a minimal risk of neurotoxic interference—a critical consideration for the elderly population affected by muscle wasting. While its baseline permeability is moderate, integrating advanced delivery systems, such as nanoformulations, can effectively bridge the gap between

its in silico pharmacokinetic profile and the required therapeutic concentrations in skeletal muscle [59].

Supporting this selection, the absence of predicted hepatotoxicity and the estimated oral acute toxicity (LD_{50}) values indicate a favorable in silico safety profile across the board. In line with the study's limitations, these ADMET results should be interpreted as preliminary indicators intended to guide subsequent experimental validation.

3.7. Molecular dynamics simulation.

To further evaluate the structural stability of the predicted ligand–protein interaction, the AKT1–ligand complex identified as the top-ranked target in the PPI network analysis was subjected to MD simulations. Simulations were performed for 300 ns to examine the stability of ligand binding within the AKT1 active site. Curcumin, which exhibited the most favorable docking score among the screened compounds, was selected for comparison with the native AKT1 ligand as a reference. Structural stability and dynamic behavior were evaluated using RMSD, SASA, and RMSF analyses (Figure 8).

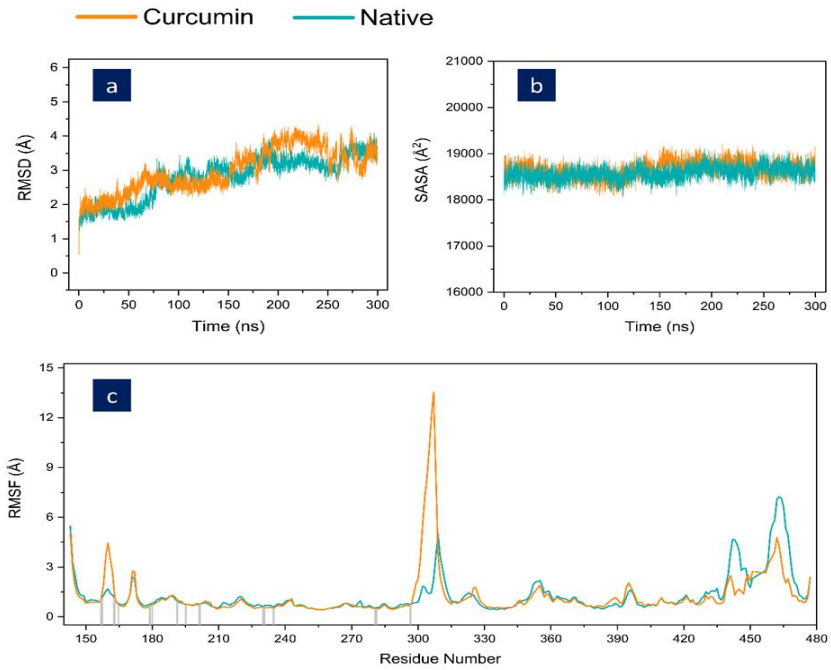

Figure 8. Structural analysis of AKT1–ligand complexes. **(a)** Backbone RMSD profiles showing structural stability over the simulation time; **(b)** SASA analysis reflecting protein surface exposure during the simulation; **(c)** RMSF of individual residues, where grey shading indicates residues located within the ligand-binding site.

RMSD analysis revealed that the Curcumin–AKT1 complex remained stable throughout the simulation. The average backbone RMSD was 2.02 Å during the initial 50 ns and increased gradually toward the end of the simulation, with an overall average RMSD of 2.98 Å, remaining comparable to that of the native ligand-AKT1 complex. The similar RMSD profiles suggest that Curcumin maintained a stable binding pose within the active site over time.

SASA analysis revealed average values of 18.655 Å² for the Curcumin–bound complex and 18.577 Å² for the native ligand complex, with no substantial differences observed. These results suggest that ligand binding did not induce major global conformational changes in AKT1 and that the simulation duration was sufficient to sample equilibrated systems.

Residue-level flexibility was assessed using RMSF analysis. The Curcumin and native ligand exhibited comparable average RMSF values (1.23 Å and 1.24 Å, respectively). Key residues involved in ligand binding at the active site, including LEU 156, GLY 157, PHE 161, GLY 162, LYS 163, VAL 164, ALA 177, LYS 179, LEU 181, GLU 191, THR 195, GLU 198, TYR 229, ALA 230, GLU 234, GLU 278, ASN 279, MET 281, and GLY 294, remained relatively stable in both systems, indicating preservation of the binding environment.

In contrast, increased fluctuations were observed in residues LYS 158, GLY 159, THR 160, PHE 161, GLY 162, and residues 298–307 in the Curcumin-bound system. These residues form a contiguous segment corresponding to loop regions adjacent to the binding pocket. The increased flexibility likely reflects local conformational adaptability required to accommodate Curcumin and is consistent with the dynamic behavior typically observed in surface-exposed or loop regions during MD simulations. Overall, the MD results indicated that Curcumin maintains a stable binding pose within the AKT1 active site throughout the simulation period.

Despite these findings, the scope of this study is limited by its computational nature. By integrating network pharmacology, molecular docking, and MD simulations, the present work provides hypothesis-generating insights into potential ligand-target interactions. Experimental validation using *in vitro* muscle cell models and in vivo sarcopenia models will be required to confirm any regulatory effects at the molecular and cellular levels. Future studies may extend this framework through structure–activity relationships analysis, compound optimization, and multi-omics integration. Additionally, evaluating synergistic interactions among *Z. officinale*, *Curcuma sp.*, and *K. galanga* in combined formulations remains an important direction for subsequent experimental investigation.

4. Conclusions

This study investigates the anti-sarcopenic potential of *Z. officinale*, *Curcuma sp.*, and *K. galanga*, elucidating their possible mechanisms of action in preserving skeletal muscle integrity. Network pharmacology analysis identified AKT1, TP53, and BCL2 as core targets, highlighting the PI3K-Akt signaling pathway and endocrine resistance as key targets for modulation. Molecular docking revealed that Curcumin (*Curcuma sp.*) exhibited the strongest binding affinity toward AKT1, while 1-dehydro-10-gingerdione (*Z. officinale*) displayed the highest affinity for TP53 and BCL2.

MD simulations confirmed the stability of the Curcumin–AKT1 complex, which maintained a trajectory comparable to the native-AKT1 complex (average RMSD backbone profile of 2.98 Å, SASA of 18.655 $Å^2$, and RMSF of 1.23 Å). Subsequent pharmacokinetic evaluations demonstrated that the prioritized compounds possess favorable drug-likeness and safety profiles, characterized by high predicted intestinal (82.19–91.757%) and moderate metabolic clearance. Notably, while Curcumin's profile suggests potential as a lead compound, its recognized bioavailability challenges highlight the need for advanced formulation strategies.

Collectively, these in silico findings suggest a multi-target therapeutic mechanism relevant to sarcopenia. However, experimental validation using *in vitro* muscle cell assays and *in vivo* models is essential to confirm regulatory effects at the cellular level. Future studies should also prioritize exploring the synergistic potential of combinatorial formulations of these herbs to maximize muscle preservation. This work provides a foundational framework for developing standardized, synergistic herbal therapies for the management of sarcopenia.

Author Contributions

Conceptualization, F.A.I., A., F., I.R.K., D.W., T.A., E.E.P., N.B.N. and M.R.I.; methodology, F.A.I., A., F., I.R.K., D.W., T.A., E.E.P., N.B.N. and M.R.I.; software, F.A.I.; validation, F.A.I., A., F., I.R.K., D.W., T.A., E.E.P., N.B.N. and M.R.I.; formal analysis, F.A.I. and A.; investigation, F.A.I. and A.; resources, F., I.R.K., D.W., T.A., E.E.P. and N.B.N.; data curation, F.A.I. and A.; writing—original draft preparation, F.A.I. and A.; writing—review and editing, F. and M.R.I.; visualization, F.A.I. and A.; supervision, F. and M.R.I.; project administration, F. and M.R.I. All authors have read and agreed to the published version of the manuscript.

Institutional Review Board Statement

Not applicable.

Informed Consent Statement

Not applicable.

Data Availability Statement

Data supporting the findings of this study are available upon reasonable request from the corresponding author.

Funding

This research was funded by [National Research and Innovation Agency (BRIN) Indonesia], grant number [6/III.9/HK/2025].

Acknowledgments

The first author wishes to express sincere gratitude to the National Research and Innovation Agency (BRIN) Indonesia, especially to all members of the Drug Design and Discovery Research Group, who facilitated the execution of this research project.

Conflicts of Interest

The authors declare no conflict of interest.

Abbreviations

The following abbreviations are used in this manuscript:

Abbreviation	Definition
ADMET	Absorption, Distribution, Metabolism, Excretion, and Toxicity
SMILES	Simplified Molecular Input Line Entry System
PPI	Protein–Protein Interaction
GO	Gene Ontology
MF	Molecular Function
BP	Biological Process
CC	Cellular Component
KEGG	Kyoto Encyclopedia of Genes and Genomes
FDR	False Discovery Rate
MVD	Molegro Virtual Docker
PDB	Protein Data Bank
MMFF94	Merck Molecular Force Field 94

Abbreviation	Definition
HIA	Human Intestinal Absorption
VD_{ss}	Steady-State Volume of Distribution
BBB	Blood–Brain Barrier
MD	Molecular Dynamics
HPC	High-Performance Computing
PBC	Periodic Boundary Condition
RMSD	Root Mean Square Deviation
SASA	Solvent-Accessible Surface Area
RMSF	Root Mean Square Fluctuation
AKT1	Alpha Serine/Threonine Kinase 1
TP53	Tumor Protein p53
BCL2	B-Cell Lymphoma 2
LD_{50}	Lethal Dose 50%

References

1. Bilski, J.; Pierzchalski, P.; Szczepanik, M.; Bonior, J.; Zoladz, J.A. Multifactorial Mechanism of Sarcopenia and Sarcopenic Obesity. Role of Physical Exercise, Microbiota and Myokines. *Cells* **2022**, *11*, 160, https://doi.org/10.3390/cells11010160.
2. Dalle, S.; Rossmeislova, L.; Koppo, K. The Role of Inflammation in Age-Related Sarcopenia. *Front. Physiol.* **2017**, *8*, 1045, https://doi.org/10.3389/fphys.2017.01045.
3. Lian, D.; Chen, M.-M.; Wu, H.; Deng, S.; Hu, X. The Role of Oxidative Stress in Skeletal Muscle Myogenesis and Muscle Disease. *Antioxidants* **2022**, *11*, 755, https://doi.org/10.3390/antiox11040755.
4. Chen, C.; Liao, D.-M. Sarcopenia, Frailty and Fall Risk-Narrative Review. *Int. J. Gerontol.* **2023**, *17*, 149–152, https://doi.org/10.6890/IJGE.202307_17(3).0001.
5. Weng, S.-E.; Huang, Y.-W.; Tseng, Y.-C.; Peng, H.-R.; Lai, H.-Y.; Akishita, M.; Arai, H.; Hsiao, F.-Y.; Chen, L.-K. The Evolving Landscape of Sarcopenia in Asia: A Systematic review and meta-analysis following the 2019 Asian working group for sarcopenia (AWGS) diagnostic criteria. *Arch. Gerontol. Geriatr.* **2025**, *128*, 105596, https://doi.org/10.1016/j.archger.2024.105596.
6. Nations, U. *World Population Ageing 2017* Department of Economic and Social Affairs Population Division: New York, **2017**; pp. 1-110.
7. Basham, S.A.; Waldman, H.S.; Krings, B.M.; Lamberth, J.; Smith, J.W.; McAllister, M.J. Effect of Curcumin Supplementation on Exercise-Induced Oxidative Stress, Inflammation, Muscle Damage, and Muscle Soreness. *J. Diet. Suppl.* **2020**, *17*, 401-414, https://doi.org/10.1080/19390211.2019.1604604.
8. Ding, K.; Jiang, W.; Zhangwang, J.; Wang, Y.; Zhang, J.; Lei, M. The potential of traditional herbal active ingredients in the treatment of sarcopenia animal models: focus on therapeutic effects and mechanisms. *Naunyn-Schmiedeberg's Arch. Pharmacol.* **2023**, *396*, 3483-3501, https://doi.org/10.1007/s00210-023-02639-7.
9. Novakovic, S.; Jakovljevic, V.; Jovic, N.; Andric, K.; Milinkovic, M.; Anicic, T.; Pindovic, B.; Kareva, E.N.; Fisenko, V.P.; Dimitrijevic, A.; Jovic, J.J. Exploring the Antioxidative Effects of Ginger and Cinnamon: A Comprehensive Review of Evidence and Molecular Mechanisms Involved in Polycystic Ovary Syndrome (PCOS) and Other Oxidative Stress-Related Disorders. *Antioxidants* **2024**, *13*, 392, https://doi.org/10.3390/antiox13040392.
10. Hattori, S.; Omi, N.; Yang, Z.; Nakamura, M.; Ikemoto, M. Effect of ginger extract ingestion on skeletal muscle glycogen contents and endurance exercise in male rats. *Phys. Act. Nutr.* **2021**, *25*, 15-19, https://doi.org/10.20463/pan.2021.0010.
11. Vargas-Mendoza, N.; Madrigal-Santillán, E.; Álvarez-González, I.; Madrigal-Bujaidar, E.; Anguiano-Robledo, L.; Aguilar-Faisal, J.L.; Morales-Martínez, M.; Delgado-Olivares, L.; Rodríguez-Negrete, E.V.; Morales-González, Á.; Morales-González, J.A. Phytochemicals in Skeletal Muscle Health: Effects of Curcumin (from *Curcuma longa Linn*) and Sulforaphane (from *Brassicaceae)* on Muscle Function, Recovery and Therapy of Muscle Atrophy. *Plants* **2022**, *11*, 2517, https://doi.org/10.3390/plants11192517.
12. Wang, S.-Y.; Zhao, H.; Xu, H.-T.; Han, X.-D.; Wu, Y.-S.; Xu, F.-F.; Yang, X.-B.; Göransson, U.; Liu, B. *Kaempferia galanga* L.: Progresses in Phytochemistry, Pharmacology, Toxicology and Ethnomedicinal Uses. *Front. Pharmacol.* **2021**, *12*, 675350, https://doi.org/10.3389/fphar.2021.675350.

13. Noor, F.; Tahir ul Qamar, M.; Ashfaq, U.A.; Albutti, A.; Alwashmi, A.S.S.; Aljasir, M.A. Network Pharmacology Approach for Medicinal Plants: Review and Assessment. *Pharmaceuticals* **2022**, *15*, 572, https://doi.org/10.3390/ph15050572.
14. Agu, P.C.; Afiukwa, C.A.; Orji, O.U.; Ezeh, E.M.; Ofoke, I.H.; Ogbu, C.O.; Ugwuja, E.I.; Aja, P.M. Molecular docking as a tool for the discovery of molecular targets of nutraceuticals in diseases management. *Sci. Rep.* **2023**, *13*, 13398, https://doi.org/10.1038/s41598-023-40160-2.
15. Aslan, Z.; Yılmaz, E.; Pulat, N.; Şeker, A.; Ertem, A.; Demirhan, M.; Gündoğdu, S.; Arslan, M.; Demir, Y. Isoindole-1,3-Dione Sulfonamides as Potent Inhibitors of Glucosidase, Aldose Reductase, and Tyrosinase: A Molecular Docking and Enzyme Inhibition Study. *Biotechnol. Appl. Biochem.* **2025**, *72*, 1517-1527, https://doi.org/10.1002/bab.2756.
16. Hollingsworth, S.A.; Dror, R.O. Molecular Dynamics Simulation for All. *Neuron* **2018**, *99*, 1129–1143, https://doi.org/10.1016/j.neuron.2018.08.011.
17. Ishfaq, M.; Hu, W.; Hu, Z.; Guan, Y.; Zhang, R. A review of nutritional implications of bioactive compounds of Ginger (Zingiber officinale Roscoe), their biological activities and nano-formulations. *Ital. J. Food Sci.* **2022**, *34*, 1-12, https://doi.org/10.15586/ijfs.v34i3.2212.
18. Shaukat, M.N.; Nazir, A.; Fallico, B. Ginger Bioactives: A Comprehensive Review of Health Benefits and Potential Food Applications. *Antioxidants* **2023**, *12*, 2015, https://doi.org/10.3390/antiox12112015.
19. Sueth-Santiago, V.; Moraes, J.d.B.B.; Sobral Alves, E.S.; Vannier-Santos, M.A.; Freire-de-Lima, C.G.; Castro, R.N.; Mendes-Silva, G.P.; Del Cistia, C.d.N.; Magalhães, L.G.; Andricopulo, A.D.; Sant´Anna, C.M.R.; Decoté-Ricardo, D.; Freire de Lima, M.E. The Effectiveness of Natural Diarylheptanoids against *Trypanosoma cruzi*: Cytotoxicity, Ultrastructural Alterations and Molecular Modeling Studies. *PLOS ONE* **2016**, *11*, e0162926, https://doi.org/10.1371/journal.pone.0162926.
20. Jantan, I.; Saputri, F.C.; Qaisar, M.N.; Buang, F. Correlation between Chemical Composition of *Curcuma domestica* and *Curcuma xanthorrhiza* and Their Antioxidant Effect on Human Low-Density Lipoprotein Oxidation. *Evid. -Based Complementary Altern. Med.* **2012**, *2012*, 438356, https://doi.org/10.1155/2012/438356.
21. Muzzazinah, M.; Yunus, A.; Rinanto, Y.; Suherlan, Y.; Ramli, M.; Putri, D.S.; Ningtyas, D.W.; Rahma, A.L.; Nabila, S.J. Profile of chemical compounds and potency of galangal (*Kaempferia galanga* L.) essential oils from Kemuning Village, Karanganyar District, Central Java, Indonesia. *Biodiversitas* **2024**, *25*, 1386–1393, https://doi.org/10.13057/biodiv/d250406.
22. Vidya, V.R.; Pillai, P.; Preetha, T.S. COMPARATIVE CHEMICAL PROFILING OF ESSENTIAL OIL COMPONENTS USING GC-MS IN MICRO, MINI AND MOTHER RHIZOMES OF KAEMPFERIA GALANGA L. *J. Adv. Sci. Res.* **2022**, *13*, 188–199, https://doi.org/10.55218/JASR.202213121.
23. Daina, A.; Zoete, V. Testing the predictive power of reverse screening to infer drug targets, with the help of machine learning. *Commun. Chem.* **2024**, *7*, 105, https://doi.org/10.1038/s42004-024-01179-2.
24. Pogodin, P.V.; Lagunin, A.A.; Filimonov, D.A.; Poroikov, V.V. PASS Targets: Ligand-based multi-target computational system based on a public data and naïve Bayes approach. *SAR QSAR Environ. Res.* **2015**, *26*, 783-793, https://doi.org/10.1080/1062936X.2015.1078407.
25. Kuhn, M.; von Mering, C.; Campillos, M.; Jensen, L.J.; Bork, P. STITCH: interaction networks of chemicals and proteins. *Nucleic Acids Res.* **2008**, *36*, D684-D688, https://doi.org/10.1093/nar/gkm795.
26. Stelzer, G.; Rosen, N.; Plaschkes, I.; Zimmerman, S.; Twik, M.; Fishilevich, S.; Stein, T.I.; Nudel, R.; Lieder, I.; Mazor, Y.; Kaplan, S.; Dahary, D.; Warshawsky, D.; Guan-Golan, Y.; Kohn, A.; Rappaport, N.; Safran, M.; Lancet, D. The GeneCards Suite: From Gene Data Mining to Disease Genome Sequence Analyses. *Curr. Protoc. Bioinform.* **2016**, *54*, 1.30.31-31.30.33, https://doi.org/10.1002/cpbi.5.
27. Szklarczyk, D.; Kirsch, R.; Koutrouli, M.; Nastou, K.; Mehryary, F.; Hachilif, R.; Gable, A.L.; Fang, T.; Doncheva, N.T.; Pyysalo, S.; Bork, P.; Jensen, L.J.; von Mering, C. The STRING database in 2023: protein–protein association networks and functional enrichment analyses for any sequenced genome of interest. *Nucleic Acids Res.* **2023**, *51*, D638-D646, https://doi.org/10.1093/nar/gkac1000.
28. Venny. Available online: https://bioinfogp.cnb.csic.es/tools/venny/ (accessed on 11 February **2025**).
29. Shannon, P.; Markiel, A.; Ozier, O.; Baliga, N.S.; Wang, J.T.; Ramage, D.; Amin, N.; Schwikowski, B.; Ideker, T. Cytoscape: A Software Environment for Integrated Models of Biomolecular Interaction Networks. *Genome Res.* **2003**, *13*, 2498–2504, https://doi.org/10.1101/gr.1239303.
30. Ge, S.X.; Jung, D.; Yao, R. ShinyGO: a graphical gene-set enrichment tool for animals and plants. *Bioinformatics* **2020**, *36*, 2628–2629, https://doi.org/10.1093/bioinformatics/btz931.

31. Li, X.; Wen, Z.; Si, M.; Jia, Y.; Liu, H.; Zheng, Y.; Ma, D. Exploration of Hanshi Zufei prescription for treatment of COVID-19 based on network pharmacology. *Chin. Herb. Med.* **2022**, *14*, 294-302, https://doi.org/10.1016/j.chmed.2021.06.006.
32. Thomsen, R.; Christensen, M.H. MolDock: A New Technique for High-Accuracy Molecular Docking. *J. Med. Chem.* **2006**, *49*, 3315–3321, https://doi.org/10.1021/jm051197e.
33. Berman, H.M.; Westbrook, J.; Feng, Z.; Gilliland, G.; Bhat, T.N.; Weissig, H.; Shindyalov, I.N.; Bourne, P.E. The Protein Data Bank. *Nucleic Acids Res.* **2000**, *28*, 235-242, https://doi.org/10.1093/nar/28.1.235.
34. Kim, S.; Bolton, E.E. PubChem: A Large-Scale Public Chemical Database for Drug Discovery. In Open Access Databases and Datasets for Drug Discovery; Daina, A., Przewosny, M., Zoete, V., Eds.; John Wiley & Sons: **2024**; pp. 39-66, https://doi.org/10.1002/9783527830497.ch2.
35. Halgren, T.A. Merck molecular force field. I. Basis, form, scope, parameterization, and performance of MMFF94. *J. Comput. Chem.* **1996**, *17*, 490–519, https://doi.org/10.1002/(SICI)1096-987X(199604)17:5/6%3C490::AID-JCC1%3E3.0.CO;2-P.
36. BIOVIA, Discovery Studio. Available online: https://www.3ds.com/products/biovia/discovery-studio (accessed on 18 February **2025**).
37. Fu, L.; Shi, S.; Yi, J.; Wang, N.; He, Y.; Wu, Z.; Peng, J.; Deng, Y.; Wang, W.; Wu, C.; Lyu, A.; Zeng, X.; Zhao, W.; Hou, T.; Cao, D. ADMETlab 3.0: an updated comprehensive online ADMET prediction platform enhanced with broader coverage, improved performance, API functionality and decision support. *Nucleic Acids Res.* **2024**, *52*, W422-W431, https://doi.org/10.1093/nar/gkae236.
38. Pires, D.E.V.; Blundell, T.L.; Ascher, D.B. pkCSM: Predicting Small-Molecule Pharmacokinetic and Toxicity Properties Using Graph-Based Signatures. *J. Med. Chem.* **2015**, *58*, 4066-4072, https://doi.org/10.1021/acs.jmedchem.5b00104.
39. Berendsen, H.J.C.; van der Spoel, D.; van Drunen, R. GROMACS: A message-passing parallel molecular dynamics implementation. *Comput. Phys. Commun.* **1995**, *91*, 43–56, https://doi.org/10.1016/0010-4655(95)00042-E.
40. Huang, J.; Rauscher, S.; Nawrocki, G.; Ran, T.; Feig, M.; de Groot, B.L.; Grubmüller, H.; MacKerell, A.D. CHARMM36m: an improved force field for folded and intrinsically disordered proteins. *Nat. Methods* **2017**, *14*, 71-73, https://doi.org/10.1038/nmeth.4067.
41. Jorgensen, W.L.; Chandrasekhar, J.; Madura, J.D.; Impey, R.W.; Klein, M.L. Comparison of simple potential functions for simulating liquid water. *J. Chem. Phys.* **1983**, *79*, 926-935, https://doi.org/10.1063/1.445869.
42. Vanommeslaeghe, K.; Hatcher, E.; Acharya, C.; Kundu, S.; Zhong, S.; Shim, J.; Darian, E.; Guvench, O.; Lopes, P.; Vorobyov, I.; Mackerell Jr, A.D. CHARMM general force field: A force field for drug-like molecules compatible with the CHARMM all-atom additive biological force fields. *J. Comput. Chem.* **2010**, *31*, 671-690, https://doi.org/10.1002/jcc.21367.
43. Yu, W.; He, X.; Vanommeslaeghe, K.; MacKerell Jr, A.D. Extension of the CHARMM general force field to sulfonyl-containing compounds and its utility in biomolecular simulations. *J. Comput. Chem.* **2012**, *33*, 2451-2468, https://doi.org/10.1002/jcc.23067.
44. El Hassab, M.A.; Ibrahim, T.M.; Al-Rashood, S.T.; Alharbi, A.; Eskandrani, R.O.; Eldehna, W.M. In silico identification of novel SARS-COV-2 2′-O-methyltransferase (nsp16) inhibitors: structure-based virtual screening, molecular dynamics simulation and MM-PBSA approaches. *J. Enzyme Inhib. Med. Chem.* **2021**, *36*, 727-736, https://doi.org/10.1080/14756366.2021.1885396.
45. Chen, X.; Wang, Y.; Liu, M.; Song, X.; Wang, D.; Zhang, J. Network pharmacology-based analysis of the effects of puerarin on sarcopenia. *Ann. Transl. Med.* **2022**, *10*, 671, https://doi.org/10.21037/atm-22-2360.
46. Damluji, A.A.; Alfaraidhy, M.; AlHajri, N.; Rohant, N.N.; Kumar, M.; Al Malouf, C.; Bahrainy, S.; Ji Kwak, M.; Batchelor, W.B.; Forman, D.E.; Rich, M.W.; Kirkpatrick, J.; Krishnaswami, A.; Alexander, K.P.; Gerstenblith, G.; Cawthon, P.; deFilippi, C.R.; Goyal, P. Sarcopenia and Cardiovascular Diseases. *Circulation* **2023**, *147*, 1534-1553, https://doi.org/10.1161/CIRCULATIONAHA.123.064071.
47. Dabur, R.; Yadav, A. Programmed Cell Death and its Implications for Skeletal Muscle Wasting. *Indian J. Clin. Biochem.* **2026**, *41*, 31-41, https://doi.org/10.1007/s12291-024-01223-x.
48. Memme, J.M.; Oliveira, A.N.; Hood, D.A. p53 regulates skeletal muscle mitophagy and mitochondrial quality control following denervation-induced muscle disuse. *J. Biol. Chem.* **2022**, *298*, 101540, https://doi.org/10.1016/j.jbc.2021.101540.
49. Hong, S.-h.; Choi, K.M. Sarcopenic Obesity, Insulin Resistance, and Their Implications in Cardiovascular and Metabolic Consequences. *Int. J. Mol. Sci.* **2020**, *21*, 494, https://doi.org/10.3390/ijms21020494.

50. Chen, H.; Huang, X.; Dong, M.; Wen, S.; Zhou, L.; Yuan, X. The Association Between Sarcopenia and Diabetes: From Pathophysiology Mechanism to Therapeutic Strategy. *Diabetes Metab. Syndr. Obes.* **2023**, *16*, 1541–1554, https://doi.org/10.2147/DMSO.S410834.
51. Barclay, R.D.; Burd, N.A.; Tyler, C.; Tillin, N.A.; Mackenzie, R.W. The Role of the IGF-1 Signaling Cascade in Muscle Protein Synthesis and Anabolic Resistance in Aging Skeletal Muscle. *Front. Nutr.* **2019**, *6*, 146, https://doi.org/10.3389/fnut.2019.00146.
52. Sun, J.; Liu, H.; Yan, Y.; Fang, F. Quercetin prevents sarcopenia by reversing oxidative stress and mitochondrial damage. *J. Mol. Histol.* **2025**, *56*, 133, https://doi.org/10.1007/s10735-025-10411-9.
53. González-Hedström, D.; Priego, T.; Amor, S.; de la Fuente-Fernández, M.; Martín, A.I.; López-Calderón, A.; Inarejos-García, A.M.; García-Villalón, Á.L.; Granado, M. Olive Leaf Extract Supplementation to Old Wistar Rats Attenuates Aging-Induced Sarcopenia and Increases Insulin Sensitivity in Adipose Tissue and Skeletal Muscle. *Antioxidants* **2021**, *10*, 737, https://doi.org/10.3390/antiox10050737.
54. Sharif Siam, M.K.; Sarker, A.; Sayeem, M.M.S. *In silico* drug design and molecular docking studies targeting Akt1 (RAC-alpha serine/threonine-protein kinase) and Akt2 (RAC-beta serine/threonine-protein kinase) proteins and investigation of CYP (cytochrome P450) inhibitors against MAOB (monoamine oxidase B) for OSCC (oral squamous cell carcinoma) treatment. *J. Biomol. Struct. Dyn.* **2021**, *39*, 6467–6479, https://doi.org/10.1080/07391102.2020.1802335.
55. More-Adate, P.; Lokhande, K.B.; Shrivastava, A.; Doiphode, S.; Nagar, S.; Singh, A.; Baheti, A. Pharmacoinformatics approach for the screening of Kovidra (*Bauhinia variegata*) phytoconstituents against tumor suppressor protein in triple negative breast cancer. *J. Biomol. Struct. Dyn.* **2024**, *42*, 4263-4282, https://doi.org/10.1080/07391102.2023.2219744.
56. Gowtham, H.G.; Ahmed, F.; Anandan, S.; Shivakumara, C.S.; Bilagi, A.; Pradeep, S.; Shivamallu, C.; Shati, A.A.; Alfaifi, M.Y.; Elbehairi, S.E.I.; Achar, R.R.; Silina, E.; Stupin, V.; Murali, M.; Kollur, S.P. *In Silico* Computational Studies of Bioactive Secondary Metabolites from *Wedelia trilobata* against Anti-Apoptotic B-Cell Lymphoma-2 (Bcl-2) Protein Associated with Cancer Cell Survival and Resistance. *Molecules* **2023**, *28*, 1588, https://doi.org/10.3390/molecules28041588.
57. Holcomb, M.; Chang, Y.-T.; Goodsell, D.S.; Forli, S. Evaluation of AlphaFold2 structures as docking targets. *Protein Sci.* **2023**, *32*, e4530, https://doi.org/10.1002/pro.4530.
58. Singh, S.P.; Deb, C.R.; Ahmed, S.U.; Saratchandra, Y.; Konwar, B.K. Molecular docking simulation analysis of the interaction of dietary flavonols with heat shock protein 90. *J. Biomed. Res.* **2016**, *30*, 67–74, https://doi.org/10.7555/JBR.30.20130158.
59. Zou, L.; Zheng, B.; Zhang, R.; Zhang, Z.; Liu, W.; Liu, C.; Xiao, H.; McClements, D.J. Food-grade nanoparticles for encapsulation, protection and delivery of curcumin: comparison of lipid, protein, and phospholipid nanoparticles under simulated gastrointestinal conditions. *RSC Adv.* **2016**, *6*, 3126-3136, https://doi.org/10.1039/c5ra22834d.

Publisher's Note & Disclaimer